

**CAAP Quarterly Report**  
**June 30<sup>th</sup>, 2025**

*Project Name:* Development of a Framework for Assessing Cathodic Protection (CP) Effectiveness in Pipelines Based on Artificial Intelligence (AI)

*Contract Number:* 693JK32350005CAAP

*Prime University:* **Texas A&M Engineering Experiment Station**

*Prepared By:* PI Homero Castaneda-Lopez Professor, [hcastaneda@tamu.edu](mailto:hcastaneda@tamu.edu),  
phone: 9794589844

*Reporting Period:* April 1<sup>st</sup> – June 30<sup>th</sup>, 2025

**Project Activities for Reporting Period:**

**Task 1. Optimizing macro/micro physical prototypes in laboratory conditions for validation of deterministic modeling.**

The validation of the developed deterministic model across both macro/micro scales is planned under laboratory conditions, focusing on two distinct cases. The first validation case is to measure the two-dimensional potential distribution within a scaled-down system incorporating various real-world factors. This system incorporates key elements such as the influence of multiple metallic structures present in the soil, anode placement, and external interferences from both DC and AC sources. The second validation case examines the impact of coating aging due to prolonged environmental exposure on the effectiveness of cathodic protection (CP). Figure 1 and Figure 2 illustrate the general design for the next stage of validation testing. By understanding these factors' influence, these validation cases seek to establish the model's accuracy in simulating the potential distribution under diverse operational scenarios.

Figure 1a display a numerical simulation of two-dimensional potential distribution for an arbitrary system, and Figure 1b gives a general description of the proposed physical test setup for the validation of the extension of the deterministic model to two dimensions

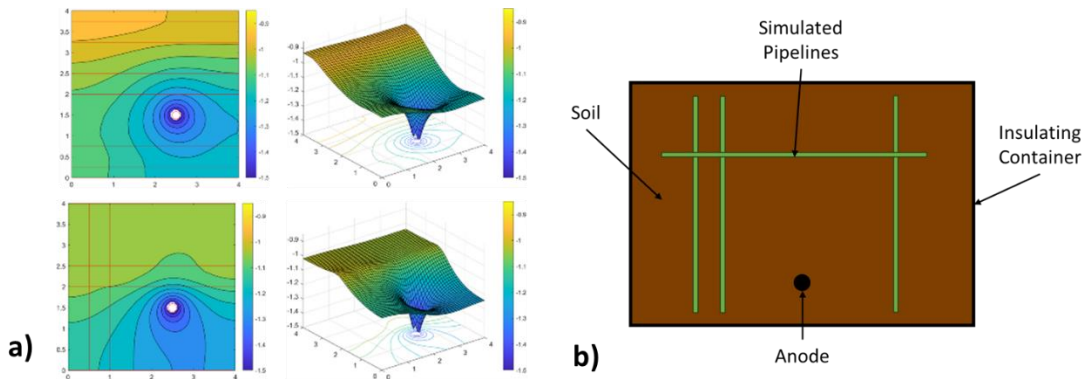


**Figure 1:** a) Numerical simulation of a two-dimensional potential distribution for an arbitrary pipeline network with singular anode placement, and b) Small scale physical model of pipeline network

Extending the model to two dimensions allows for the model to include a variety of other factors that are important when understanding the effectiveness of a CP system. Performing lab-scale validation can give confidence in the model for the extension up to the field scale with real-world systems. To create a lab-scale system, it is planned to fill an insulating container with either soil from the field or a created soil mixture. For mimicking the buried pipelines, carbon steel cylindrical samples will initially be coated with a fusion-bonded epoxy (FBE) and buried in the soil. CP can then be applied to the simulated pipeline network, and the potential distribution can be measured. The proposed system offers a high degree of customization, allowing for the characterization of various factors that influence the effectiveness of a CP system. As well as how these factors affect the detection of coating defects.

Figure 2 shows a general description of the proposed physical test setup for testing the effect of environmental exposure on various coating systems on the effectiveness of cathodic protection (CP) and electrical properties of the coating.

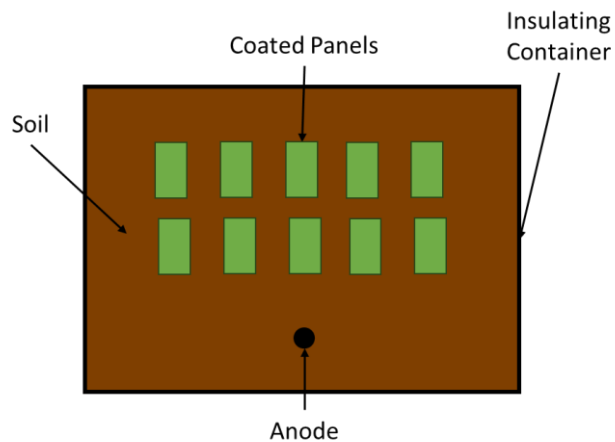


**Figure 2:** Physical setup for testing the effectiveness of CP on aged coating panels

Understanding the impact of environmental exposure on the electrochemical properties of various coating systems can be used for defining the interfacial impedance inside the deterministic model. Like the first validation case, aging of the coatings will be performed inside an insulating container containing either soil taken from the field or an artificial soil mixture created in the lab. To age the coatings, they will either be under CP or allowed to age naturally without an external potential source. This is to understand how varying levels of overpolarization can affect the electrical properties of the coating. At various time points during the aging process, the coated panels will be out from the soil and prepared for evaluation. After cleaning the coated panels, electrochemical impedance spectroscopy (EIS) will be performed on multiple locations on the panel to measure the change in the electrical properties of the coating. After EIS testing, the coated panels can then be cross-sectioned to determine the state of the metal interface under the coating. The determined electrical properties of the aged coating can then be used inside the deterministic model for simulating the buried pipelines under various aging conditions.

**Task 2: Integrating field inspection, theoretical, with experimental data by applying pattern recognition techniques relating the pipeline-coating-soil system with CP.**

## Proposed framework

The transmission-line model (TLM) was developed by the Texas A&M team to numerically compute the potential distribution along the soil–pipeline interface, taking into account the spatial heterogeneity. However, variability in soil resistivity, coating impedance, and other environmental factors introduces uncertainty that purely physics-based models cannot fully capture. To address this, we developed and implemented a physics-informed and uncertainty-aware Bayesian digital twin for pipeline external corrosion assessment, which couples a physics-based transmission-line model (TLM) with a Bayesian probabilistic updating framework. By integrating high-fidelity numerical simulation of the pipeline-soil interface with probabilistic inference, the digital twin yields spatially resolved predictions of coating interfacial impedance and assesses cathodic protection (CP) effectiveness, along with quantified uncertainty. The proposed approach, as shown in Figure 3, enhances traditional external corrosion direct assessment (ECDA) by accounting for heterogeneous soil and coating properties, enabling more reliable severity estimates and informed maintenance planning.

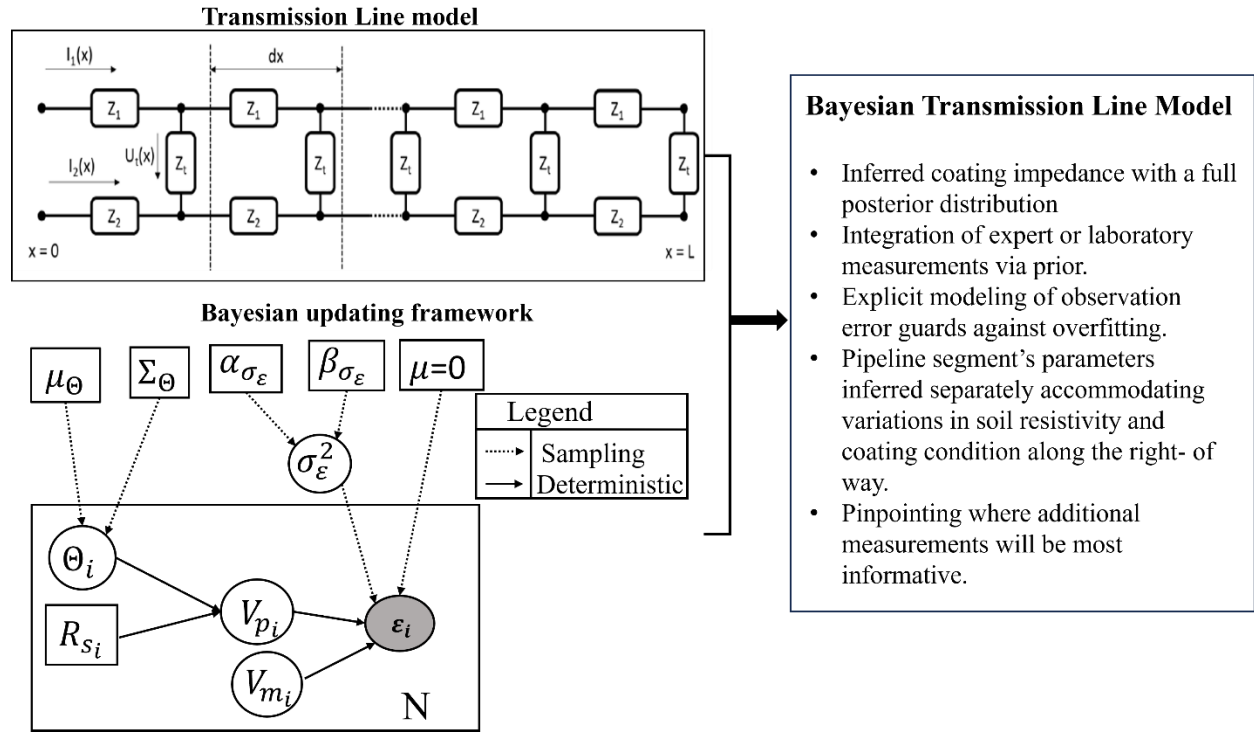


Figure 3: Proposed framework for Bayesian Transmission Line Model

## Bayesian framework

In the proposed model, known inputs include soil resistivity along the pipeline ( $R_s$ ) from soil surveys and coating resistance ( $R_c$ ) from the baseline pipeline information, CIPS voltage readings along the pipeline ( $V_m$ ), and locations of cathodic protection (CP) rectifiers ( $X_m$ ) are from CIPS readings and pipeline CP design. The primary objective is to infer the coating impedance of each pipeline segment given the CIPS survey data, as these parameters directly indicate the severity of pipeline degradation. The random variables in this model are  $R_c$  along the right-of-way and hence the model parameters vector  $\Theta = [R_c]$  is a set of coating resistances throughout the pipeline milage.

Given sampled values of the parameter vector  $\Theta$ , the predicted CP potential ( $V_p$ ) is computed using the TLM forward model. In practice, the predicted values ( $V_p$ ) rarely match the measured CIPS values ( $V_m$ ) perfectly due to model inaccuracies, environmental uncertainties, and data noise. This discrepancy is represented by an error term  $\epsilon$ , which is assumed to be independently and identically distributed as:

$$\epsilon = N(0, \sigma_\epsilon^2).$$

Since soil resistance is always positive quantity parameters are assumed to follow a lognormal distribution. According to Bayesian literature [1][2] a noninformative prior (weakly informative prior) like an inverse gamma distribution ( $\Gamma^{-1}(\alpha_{\sigma_\epsilon}, \beta_{\sigma_\epsilon})$ ) can be assumed as prior for the variance ( $\sigma_\epsilon^2$ ) of the model. Thus, the components of the Bayesian model are defined as,

$$Prior(p = (\Theta, \sigma_\epsilon)) = \prod_i^N LN(\Theta_i, \mu_{\Theta_i}, \Sigma_{\Theta_i}) \times \Gamma^{-1}(\sigma_\epsilon; \alpha_{\sigma_\epsilon}, \beta_{\sigma_\epsilon})$$

$$Likelihood(\epsilon|p) = \prod_i^N N(\epsilon; \mathbf{0}, \sigma_\epsilon^2)$$

$$post(p|\epsilon) \propto \Gamma^{-1}(\sigma_\epsilon; \alpha_{\sigma_\epsilon}, \beta_{\sigma_\epsilon}) \times \prod_i^N LN(\Theta; \mu_\Theta, \Sigma_\Theta) N(\epsilon; \mathbf{0}, \sigma_\epsilon^2)$$

where  $N$  is the number of observed data.

### **Task 3: Validation of the *a priori* framework with experimental and field conditions for characterization/modeling and Evaluation/Validation**

#### **Field data validation**

To demonstrate feasibility, we first applied our framework to a 56 km pipeline by coupling a forward Transmission Line Model (TLM) with field-measured soil resistivity profiles and using Close Interval Potential Survey (CIPS) voltages as the observed data. The pipeline was discretized into ~28 segments (2 km each), with each segment's coating resistance treated as an unknown inference parameter. We performed Bayesian inversion using the No-U-Turn Sampler (NUTS) in PyMC, yielding posterior distributions and 95 % credible intervals for each segment's impedance as shown in Figure 4. As seen in Figure 4(a), the posterior predictive mean potentials (solid line) closely track the observed CIPS voltages, capturing both the overall trend and local fluctuations. Figure 4 (b) plots the segment-wise posterior mean coating impedance (solid curve) together with 95 % credible intervals (shaded). Variability in impedance is notably low at the anode locations where concentrated CP current drives the posterior to tighten, while mid-span segments between rectifiers exhibit both lower mean impedances and wider credible intervals, flagging these zones as potential coating degradation hotspots.

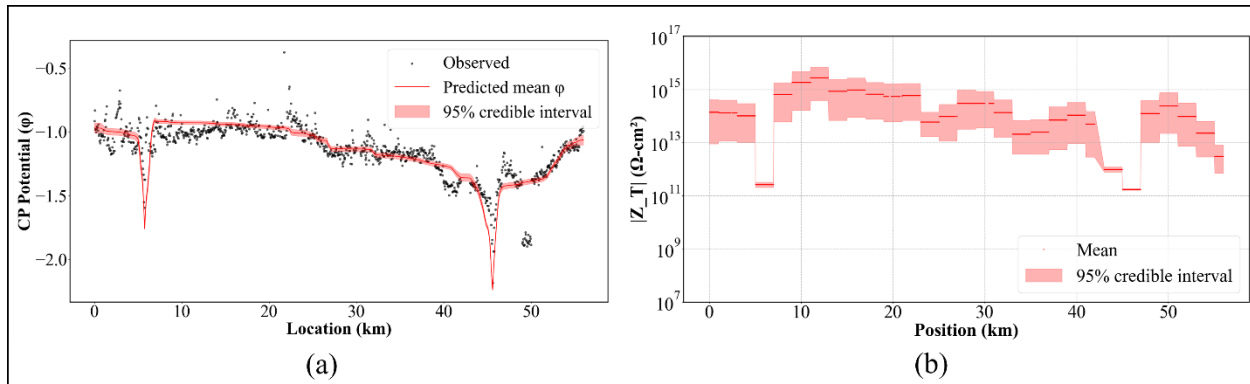


Figure 4: (a) Observed vs Predicted potential (b) Coating Impedance along pipeline right of way. Further validation was done by applying the model to a 110km pipeline as shown in Figure 5. The pipe was discretized into 2km segments again resulting in approximately double inference parameters. A major challenge in the Bayesian TLM implementation is the computational time required to sample from a high-dimensional posterior. With  $\sim 55$  coating-resistance parameters, each NUTS iteration requires solving the TLM forward model (a sparse linear system) 55 times per leapfrog step to evaluate gradients, dramatically increasing per-sample cost. Achieving adequate effective sample sizes typically demands tens of thousands of iterations, further compounding runtime.

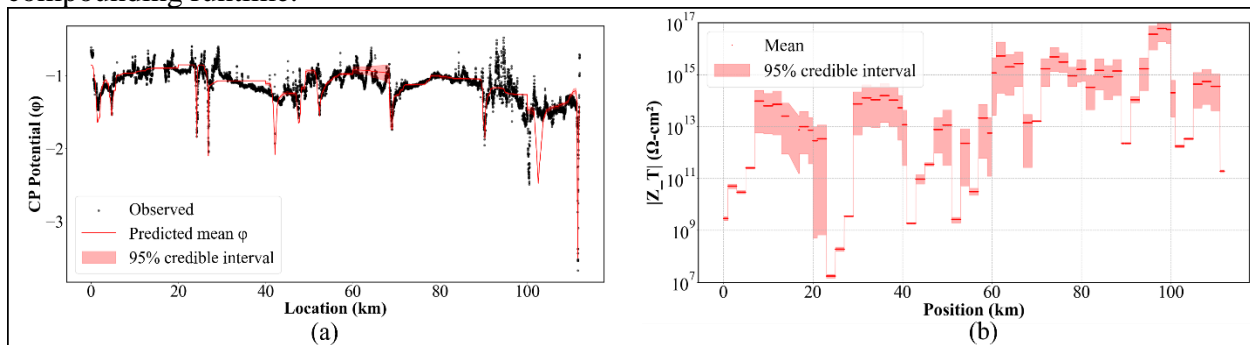


Figure 5: (a) Observed vs Predicted potential, (b) Coating Impedance along pipeline right of way. Future work will focus on replacing the current fixed 2 km segmentation with an adaptive discretization scheme that dynamically refines the mesh where it matters most. In practice, this means allowing users or an uncertainty-driven algorithm to specify regions of interest (e.g., zones with wide posterior credible intervals or suspected coating defects) and automatically subdivide those areas into shorter segments (e.g., 500 m or finer). Coarser segmentation would be retained in regions of low uncertainty to preserve computational efficiency. By coupling this adaptive mesh refinement to the Bayesian updating loop, segment granularity evolves as new CIPS data arrive, the digital twin will deliver higher-resolution impedance estimates exactly where they're needed, guide targeted inspections, and reduce unnecessary computation in benign sections of the pipeline.

#### Task 4: Procedure based on ECDA method.

External Corrosion Direct Assessment (ECDA), described by NACE standard SP0502, is an organized process to characterize and evaluate onshore steel pipeline systems. The methodology is proposed to be able to manage the risk of external corrosion failures to ferrous pipelines and prioritize the numbers and locations for repairs, and as a consequence, the integrity of the metallic

pipeline is maximized. The ECDA comprises four steps, namely: (1) pre-assessment, (2) indirect assessment, (3) direct assessment, and (4) post-assessment.

The development of the TLM-probabilistic platform will allow the preassessment step to have an a priori state of the pipelines, including remote pipelines. The development will also include a complement for the post-assessment step.

We will cover several case studies for different anomalies to test the concept in a DA method with the current database.

**Project Financial Activities Incurred during the Reporting Period:  
Project Activities with Cost Share Partners:**

During the seventh quarter of this project, we met several times (around six) with the co-sharing partners; the following outcomes from the meeting were:

- Integral Solutions facilitated the collection of databases needed in this project. We have identified

**Project Activities with External Partners:**

- We will organize a technical workshop with the team partners to get feedback on our proposal concept.
- We will organize different courses for pipeline companies, one of the topics will be integrity and risk.
- A second course for corrosion fundamentals and applications has been scheduled next month. One chapter is dedicated to Pipelines.

**Potential Project Risks:**

Currently, there are no potential risks.

**Future Project Work:**

We anticipate following the proposed timeline with no current changes during the next months.

We will follow the Gantt chart to mark the progress and plans.

During the next 30, 60, and 90 days, we will perform task 2 activities. Also, we will continue with Task 3 activities and start with Task 4 for the next 30, 60, and 90 days.

Theoretical work, laboratory work, and current database analysis will be considered for the next quarter.

- Include ways of estimating coating defects activity and severity in the coating impedance model
- Continue validating the model with multiple sets of field data.
- Simulation and characterization of stray current and interferences.

The timeline and schedule for the project are in the Gantt chart.

Task/Subtask	Fiscal Year						
	2023	2024	2025	2025	2026	2026	2026

	Q4	Q1	Q2	Q3	Q4	Q1	Q2	Q3	Q4	Q1	Q2	Q3
Task 1: Designing and building the physical prototypes in laboratory conditions and deterministic modeling												
Task 2: Integrating field inspection, theoretical, with experimental data by applying pattern recognition techniques relating the pipeline-coating-soil system with CP												
Task 3: Validation of the <i>a priori</i> framework with experimental and field conditions for characterization/modeling and Evaluation/Validation												
Task 4: Development and validation of the methodology for ECDA based on CP levels												

**Deliverable Milestones are indicated in black\*, and in dark green is the extended activities.**

### Potential Impacts to Pipeline Safety:

During the Transmission Line Modeling, we integrate the algorithms used for Artificial Intelligence. The potential impact is the results generated for the AI algorithm, the TLM is based on a deterministic and fundamental approach. This can not only show different trends for a buried structure under cathodic protection but also include several features in the RoW, resistivity, rectifier location, coating anomalies, and soil characteristics. The rectifiers, anodic beds, soil compositions, current distribution, etc. Finally, different distributions due to current leakage or impedance magnitude can lead the characterization and quantification of interferences.

### References

1. Huang, V.M.-W., et al., *The apparent constant-phase-element behavior of an ideally polarized blocking electrode: a global and local impedance analysis*. Journal of the Electrochemical Society, 2006. **154**(2): p. C81.
2. Brug, G., et al., *The analysis of electrode impedances complicated by the presence of a constant phase element*. Journal of electroanalytical chemistry and interfacial electrochemistry, 1984. **176**(1-2): p. 275-295.
3. Tsai, Y.-T. and D. Whitmore, *Nonlinear least-squares analyses of complex impedance and admittance data for solid electrolytes*. Solid state ionics, 1982. **7**(2): p. 129-139.
4. Marquardt, D.W., *An algorithm for least-squares estimation of nonlinear parameters*. Journal of the society for Industrial and Applied Mathematics, 1963. **11**(2): p. 431-441.
5. Alper, J.S. and R.I. Gelb, *Standard errors and confidence intervals in nonlinear regression: comparison of Monte Carlo and parametric statistics*. Journal of Physical Chemistry, 1990. **94**(11): p. 4747-4751.
6. Boukamp, B.A., *A nonlinear least squares fit procedure for analysis of immittance data of electrochemical systems*. Solid state ionics, 1986. **20**(1): p. 31-44.
7. Macdonald, J.R. and J. Garber, *Analysis of impedance and admittance data for solids and liquids*. Journal of the Electrochemical Society, 1977. **124**(7): p. 1022.

# Appendix

## Lab Validation

Figure shows the fitting results of the local impedance model and experimental data for coatings with thicknesses of 15 mils, 25 mils, and 35 mils. For the intact coating, it was assumed that the impedance followed that of the dual layer model coating impedance model. This model was chosen since in the high frequency domain there was a dispersion of the phase angle. For an ideal/perfect coating it would be expected for the phase angle value at high frequencies ( $>10^4$  Hz) would be  $-90^\circ$ , but the measured values are closer to  $-87^\circ - -85^\circ$ . Overall, the fitting of the model to the experimental data was able to provide reasonable values of the impedance magnitude and phase angles over the entire frequency range. The model input parameters obtained from the fitting are shown in Table , with a baseline coating resistivity value that was determined to be around  $8.4e13 \Omega\text{-cm}^2$ . Comparing the impedance magnitudes there was a good fitting between the model and the experimental data. In the lower frequency regime ( $<10^0$  Hz) there was some discrepancies between the phase angles calculated by the model and those measured by the macro-EIS measurements, but in the higher frequency ranges the model's output followed closely with the experimental data. In its entirety the local impedance model was able fit the model's input parameters to accurately fit the numerical model to the experimental data. Allowing for the determination of the coating parameters that can then be used for the other steps in the model's validation testing.

**Table 1:** Fitting parameters obtained from fitting local impedance model with intact coating experimental data with a baseline coating resistivity of  $8.4e13 \Omega\text{cm}^2$ .

Sample ID	$\delta$ <i>cm</i>	$\lambda$ <i>cm</i>	$\epsilon_r$
15 mil Intact	.0171	1.0e-3	9.5
25 mil Intact	.0254	1.8e-3	9.5
35 mil Intact	.0377	2.0e-4	8.5

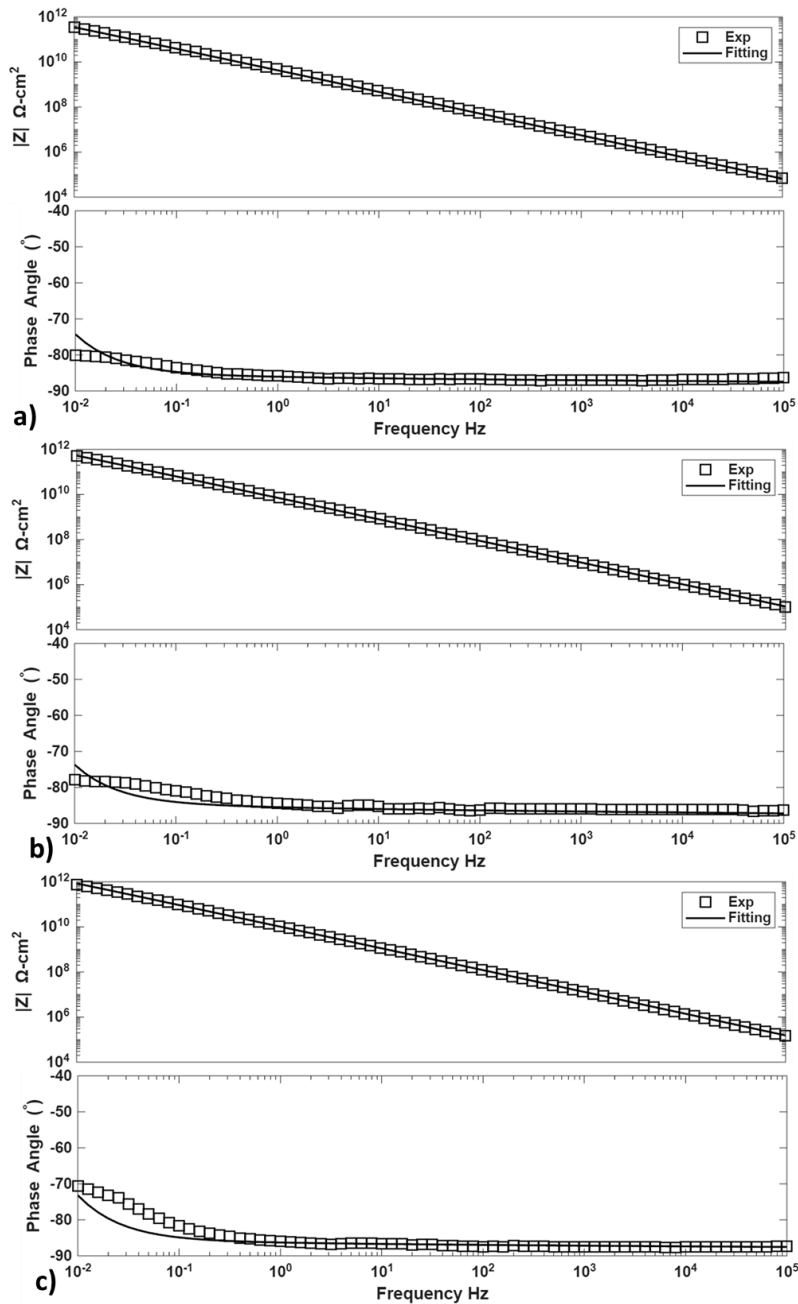


**Figure 6:** Fitting of the impedance magnitude and phase angle values generated by the model with the experimental data for a simulated intact coating with thickness of a) 15 mils, b) 25 mils, and c) 35 mils

For the heterogeneous system, it was assumed that the intact coating region had the same impedance properties as those found from fitting the model to the intact coating. Allowing for a simplification of the number of unknowns in the system and to extract information solely about the holiday introduced into the coating. To define to the interfacial impedance of the holiday it, a mixed model where a CPE element was used to describe the double layer capacitance of the system and using a mechanistic description of the charge transfer resistance. Figure and Figure show the fitting of the model for two cases. The first case was to understand the role of coating thickness on the frequency dependent impedance response of a coating with a holiday. Followed

by second case which compared the frequency dependent impedance response of coating with varying holiday sizes. The fitting parameters of the obtained for the holiday interface are shown in Table . For further comparison with traditional EIS data analysis methods the experimental data was also fitted using traditional lumped circuit EEC methods and the circuit parameters obtained are shown in Table .

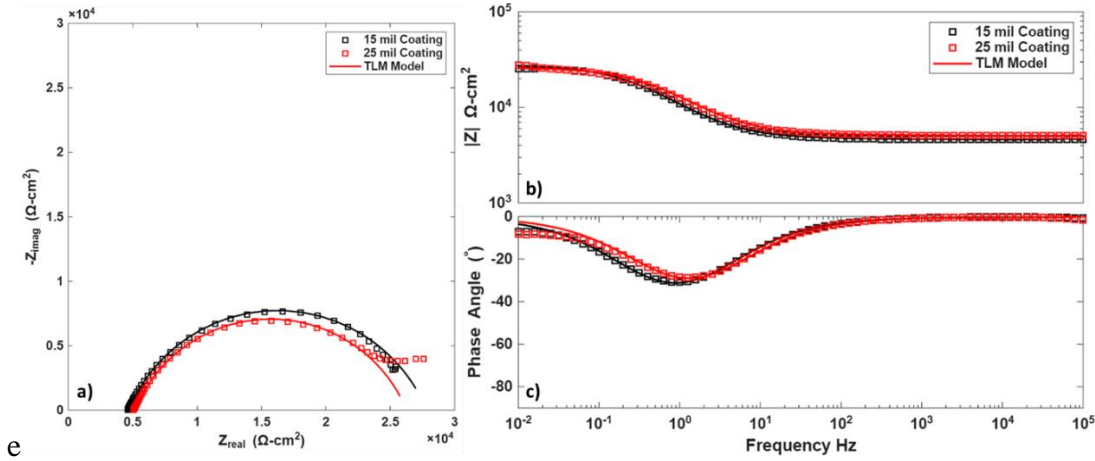


**Figure 7:** a) Nyquist, b) Bode, and c) Phase Angle plots comparing the outputs of the local impedance model for 15 mil and 25 mil coatings with a small holiday.

It becomes evident from Figure that the overall impedance response of the system seemed to be less reliant on the thickness of the coating and controlled primarily by the impedance response of the holiday. Which can be seen from the  $R_{ct}$  values obtained from fitting for the holiday region. There as only a 6% change in the obtained  $R_{ct}$  for the numerical model from the 25 mil to 15 mil samples, which could be possibly attributed to the inherent variation that is present from sample to sample. Comparing the  $R_{ct}$  values obtained from traditional fitting methods, there was a larger variation of around 28% between the 25 mil and 15 mil samples, with the 15 mil samples showing a slightly higher impedance response. This increased impedance could be attributed to the lower activity of the holiday in the 15mil sample, and the larger variation is due to the lumped circuit fitting combining the coating and holiday impedances into one overall response. Figure shows the fitting of the local impedance model to the experimental data obtained for a 25 mil coating with two holiday sizes.

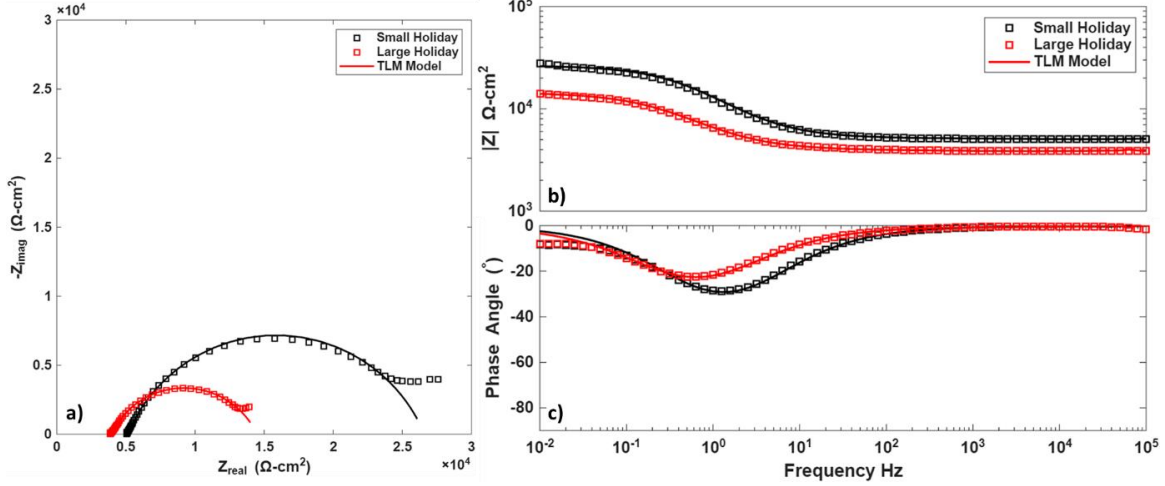


**Figure 8:** a) Nyquist, b) Bode, and c) Phase Angle plots comparing the outputs of the local impedance model for 25 mil coating with a small and large holiday.

It can be clearly seen from Figure and Figure that the influence of the holiday size on the global impedance response of the system is more pronounced compared to role of the coating thickness. Table shows that  $R_{ct}$  obtained by traditional fitting methods decreased by approximately 45% as the holiday area increased from smaller to larger holiday. Which consequently there is approximately 45% difference in exposure area between the small (0.218 cm<sup>2</sup>) and the large holiday (0.507 cm<sup>2</sup>). The difference in holiday areas can be directly linked to the decrease in the global response of the system when going from coating with the smaller holiday to the larger holiday. Additionally, the fitted  $R_{ct}$  from the numerical model had only a relatively small difference in activity between the two samples.

**Table 2:** Fitting Parameters for the holiday with resulting charge transfer resistance and CPE properties.

Sample ID	$R_{ct}$ $\Omega\text{cm}^2$	$C_{dl}$ $\mu\text{F}/\text{cm}^2$	$n$	$Q_{dl}$ $\mu\Omega^{-1}\text{s}^{-n}$
15 mil Holiday – Small	7.08E3	60.5	0.76	92.9
25 mil Holiday - Small	6.47E3	42.5	0.74	73.5
25 mil Holiday - Large	5.60E3	78.0	0.72	126.0

**Table 3:** EEC Parameters obtained from traditional lumped circuit fitting methods

Sample ID	$R_{ct}$ $\Omega\text{cm}^2$	$C_{dl}$ $\mu\text{F}/\text{cm}^2$	$n$	$Q_{dl}$ $\mu\Omega^{-1}\text{s}^{-n}\text{cm}^{-2}$
15 mil Holiday – Small	3.12e4	6.56	0.768	19.4
25 mil Holiday - Small	2.23E4	10.3	0.715	25.4
25 mil Holiday - Large	1.09E4	19.1	0.706	45.2

From the three systems that model was fit to, the obtained impedance response of the holiday showed only slight variation across the three samples. This variation most likely arises from the sample-to-sample variation that was introduced during the cutting and removal of the

coating during holiday preparation. A direct comparison of the holiday impedance parameters from the numerical model and the circuit parameters obtained by traditional fitting methods is not feasible. The numerical model analyzes each region separately, whereas the lumped circuit model only uses a single circuit to represent all processes occurring at the interface. Figure gives a better understanding of how the numerical model can effectively handle the various processes as compared to that of a lumped circuit model. Figure compares the Bode plots of the individual impedance responses and the total impedance of the numerical model output to the impedance response of the lumped circuit fitting.

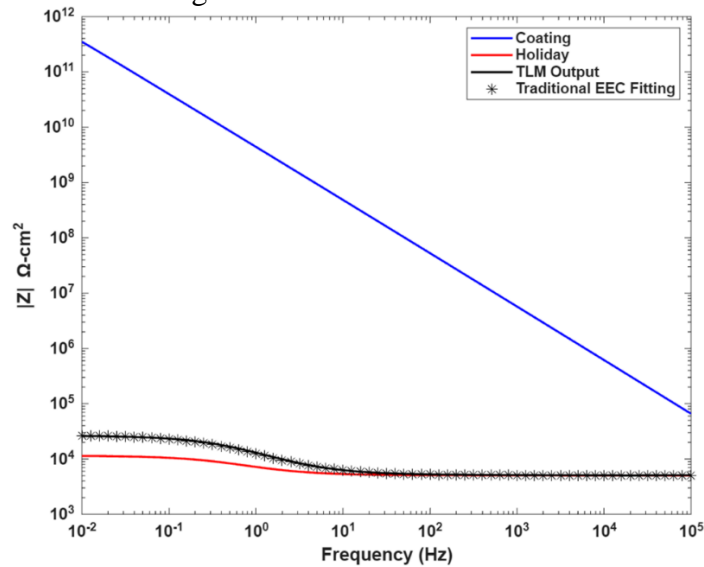


**Figure 9:** Comparison of the Bode plots for various outputs of the local impedance model and the fitting parameters obtained from traditional EEC fitting.

It is important to note that the total impedance response of the numerical model and lumped circuit model are aligned over the entire frequency range. Showing how the numerical model is a summation of all the processes occurring at the interface to create a total response of the system. It also highlights the fact that the lumped circuit model does not distinguish between the coating and holiday impedance. In the low frequency regime ( $<10^1$  Hz) the total impedance response of the system starts to differ from the holiday impedance. This likely occurs due to the increased resistive response of the coating at low frequencies, which raises the overall impedance in this region when averaged.

The final validation step for the numerical impedance model was to compare the frequency-dependent global impedance, local impedance, along local impedance distribution at a singular frequency, with LEIS measurement data. The impedance response of the defect introduced into the coating was the average of the holiday fitting parameters from Table . For modeling the coating, it was chosen to assume that the coating could be seen as an ideal coating with no variation of the physical parameters through the coating thickness. This simplification was chosen since we were dealing with a relatively thin coating ( $<100 \mu\text{m}$ ) compared to the coating thicknesses used for model validation ( $>375 \mu\text{m}$ ). Figure shows the comparison of the global and local frequency-dependent impedance response of the numerical model with the measured responses.

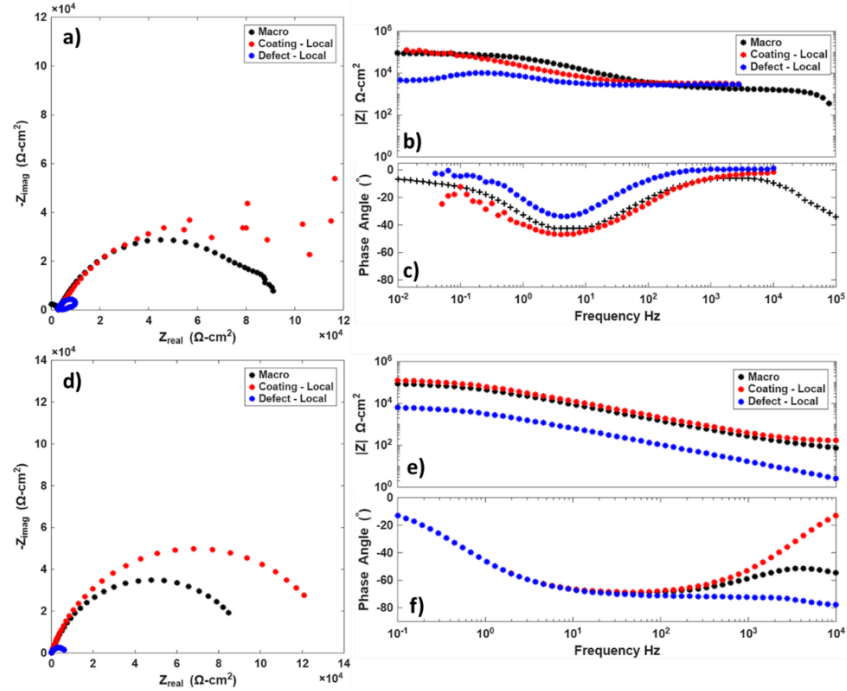


**Figure 10:** a) Nyquist, b) Bode, and c) Phase angle plots of global and local impedance obtained from experimental data, and d) Nyquist, e) Bode, and f) Phase angle plots of global and local impedance obtained from experimental data, and

Figure shows that using an ideal coating response, coupled with the fitted holiday impedance response that the numerical model was able to sufficiently model the impedance response of the damaged coating system as compared to the LEIS data. Comparing the impedance magnitude from the LEIS data and the model's output showed that they had a similar order of magnitude, and displayed very similar impedance responses between the two systems. These features are reinforced in Figure , which compares the local impedance distribution measured by the LEIS technique to the impedance distribution output of the model.

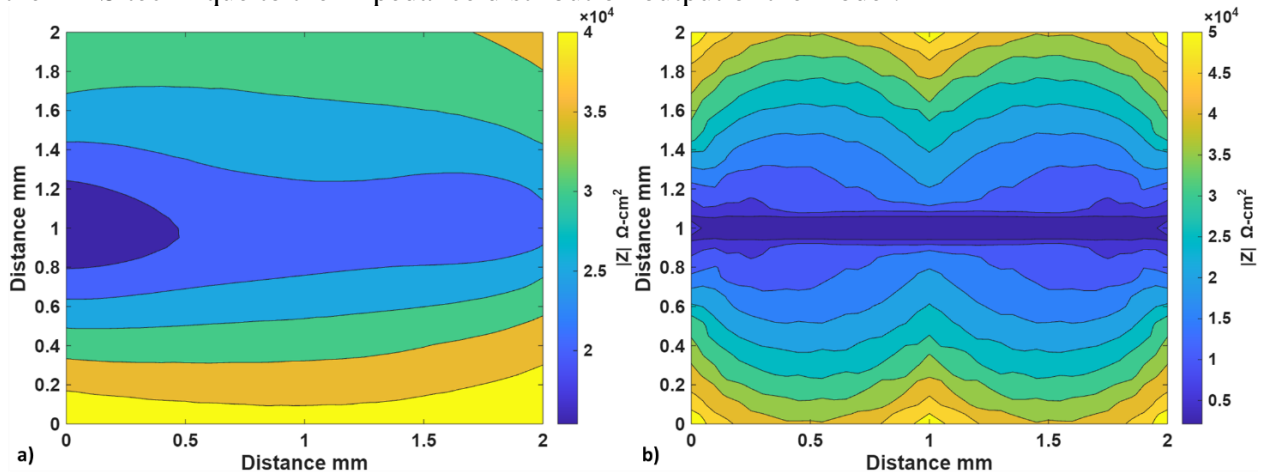


**Figure 11:** a) Measured and b) simulated local impedance distribution of electrochemical impedance in 2 mm x 2mm area at 10Hz

As was to be expected the lowest  $|Z|$  values occurred over the defect and with increasing  $|Z|$  traveling farther away from the defect towards the edges of the sample. Some of the discrepancies

between the model’s output and LEIS data could be due to a couple of features. The first assumption was that the coating was an ideal and perfect coating, which might be an invalid assumption due to the preparation of the coating needed to perform the LEIS measurements. For preparation of the coated samples for LEIS testing the coating was mechanically ground and polished to reduce the thickness of the coating to limit the separation of the substrate and probe tip. This coating preparation could cause defects or imperfections of the coating that could attribute to the deviation of from ideal impedance response. From Figure a it is evident that the impedance measured directly above the defect does not display an ideal RC/RCPE type response that was used in the mixed model for the holiday, and in the low frequency range there is a hook present that could possibly be due to more complex electrochemical reactions taking place or the adsorption of species on the surface<sup>44</sup>. In this initial iteration of the numerical model, the interfacial impedance models do not consider these complex processes since it was created for modeling the basic impedance responses of a general electrochemical interface. Comparing the impedance values over the defect in Figure a and b there was a measurable difference between the measured and simulated values. A possible explanation for the difference in measured impedances could be due to the probe height during LEIS testing. The probe height was set to 75 – 100 μm above the coating, giving a probe height above the metal substrate around 150 – 200 μm. With the larger probe height relative to the base metal, there is possible loss in the resolution when performing measurements above the defect. This decreased resolution could be a reason why there was an increase in the measured impedance magnitude since it would be measuring the signals from the defect and adjacent coating rather than solely measuring the local impedance directly above the defect.

## Laboratory Results

### Experimental Design

The experimental test matrix is shown in Table . Base metal and coating were chosen specifically selected to try and simulate the most used materials in the field. Currently all lab testing is being performed with 1018 CS base metal and fusion bonded epoxy (FBE) coating that is applied in house. With plans to include the other base metals and commercially applied coatings. The testing solution for all testing was selected to be NS4 solution with various pH values. This solution simulates the near soil environment seen in the field and consists of 4 chemicals: sodium bicarbonate (NaHCO<sub>3</sub>), potassium chloride (KCl), Calcium Chloride (CaCl<sub>2</sub>), and magnesium sulfate heptahydrate (MgSO<sub>4</sub>·7H<sub>2</sub>O). Exact composition and methods for altering pH are detailed below. The cathodic protection (CP) and coating state were varied to simulate the various conditions that in use pipelines can be found. Understanding how the CP level and coating state affect the impedance response of the system can provide more insight into detecting problems with pipelines earlier and with more accuracy.

**Table 4:** Experimental Test Matrix

Base Metal	Testing Solution	CP State (mV vs SCE)	Coating	Coating State	Coating Thickness (mil)
1010/1018	NS4 – As-recived	OCP (no protection)	Coal Tar	Intact	15
X52	NS4 – Neutral pH	-637 (under protection)	FBE	Holiday – small	20
X68	NS4 – Acidic pH	-777 (standard protection)	Yellow Jacket	Holiday – large	25
		-1227 (over protection)	Tri-layer	Delamination	35
			4500		25-40

## Test Procedure

### Laboratory Testing

1018 carbon steel plates were coated with a commercial grade FBE. The thickness of the coating varied from 10 mil to 50 mil. Coating thickness was controlled using a micrometer-adjustable film applicator. Two initial studies were performed with the FBE coatings: 1) effect of coating thickness on impedance response of the system with and without holidays at OCP, and 2) Effect of CP state for a coating with a thickness of 25 mil under the three-coating states (intact, holiday, and delamination). For the initial holiday creation, the holiday was of square geometry and was cut by hand into the coating after the coating was fully cured. The dimensions of the holiday were 0.5 cm x 0.5 cm (0.20" x 0.20"), giving a surface area of 0.25 cm<sup>2</sup> (0.039 in<sup>2</sup>). All holidays were created with a circular geometry and were cut with an endmill to ensure that the created holidays are consistent. The diameters of the small and large holidays are 0.516 cm (0.203") and 0.794 cm (0.313"), respectively. See the setup system in Figure 12.

The NS4 solution was used as the testing solution to simulate the corrosion of buried pipelines. NS4 is a soil-mimicking solution that consists of potassium chloride (0.122 g/L), sodium bicarbonate (0.483 g/L), calcium chloride (0.137 g/L), and magnesium sulfate heptahydrate (0.131 g/L). To adjust the pH of the solution, various concentrations of CO<sub>2</sub>/N<sub>2</sub> will be purged through the solution, where increasing the amount of bicarbonate in the solution lowers the pH of the solution.

All electrochemical testing was performed at ambient conditions with a three-electrode system. Where a saturated calomel electrode (SCE) was used as the reference electrode, platinum mesh as the counter electrode, and the tested material as the working electrode. EIS measurements were performed by applying a sinusoidal perturbation while varying frequencies from 100 kHz to 10 mHz. For the intact coating samples, the potential perturbation was set to 15 mV<sub>rms</sub>, and for samples with defective coatings, it was set to 10 mV<sub>rms</sub>. A large potential signal was applied to the intact coating samples to increase the current response of the system, lowering the amount of noise in the measurements. To simulate the various levels of CP, the DC bias potential for the EIS signal was set to the specified potentials.

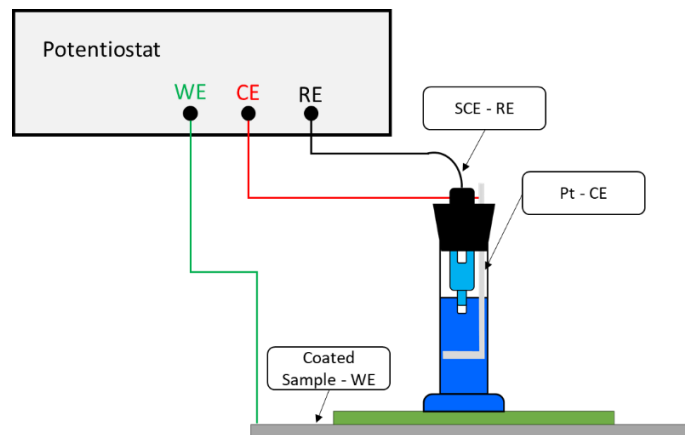


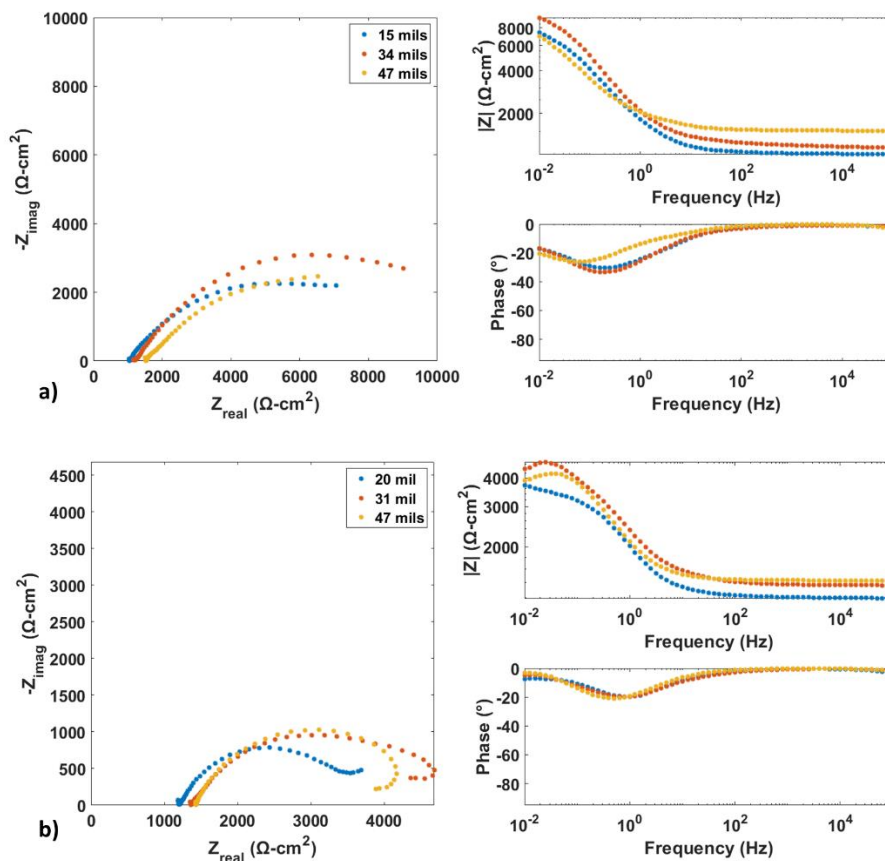
**Figure 12:** EIS testing schematic

After performing OCP, LPR, and EIS, the samples underwent decay testing. Starting with the OCP measurement, the initial potential was selected in the anodic direction of the process at +0.1V from the OCP.

## Results and Discussions

### Electrochemical Impedance Spectroscopy Study: Lab Data

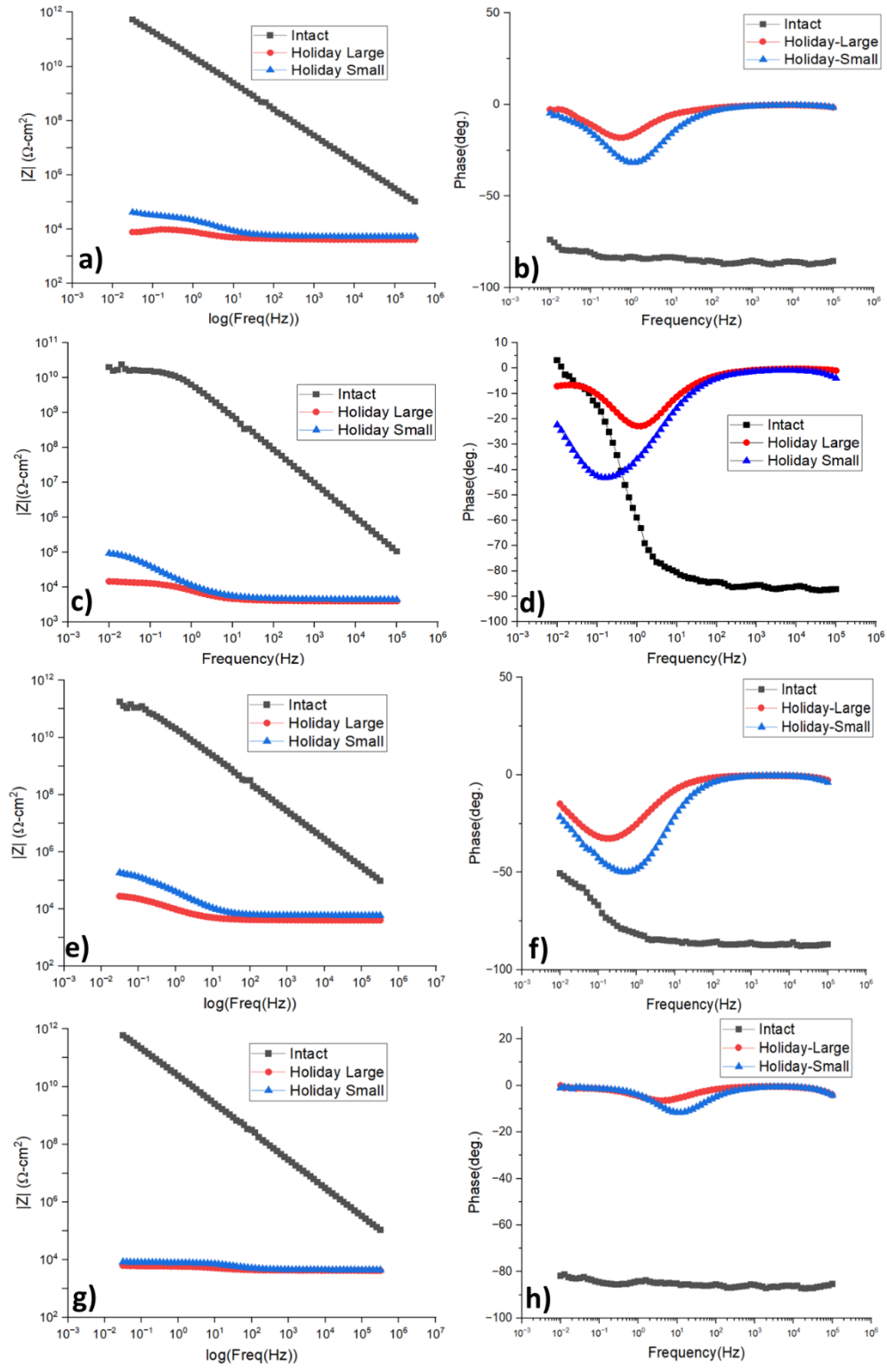
Figure 3 shows the effect of coating thickness on the impedance response of a coated substrate with two different holiday radii. For all coating thicknesses, there is little deviation in the impedance response between the three coatings for each holiday size. But it can be seen that with the smaller holiday, the overall impedance response is larger compared to the samples with the larger holiday for all coating thicknesses.



**Figure 3:** Effect of coating thickness on the impedance response of a coated substrate with a) 0.516 cm and b) 0.794 cm holiday

Figure 4 shows the effect of polarization condition on the impedance response of FBE coatings with and without holidays present in the coating. At all potential values, intact coating shows consistently high impedance ( $10^{10}$ - $10^{12}$   $\Omega\text{-cm}^2$ ) at low frequencies, with a linear decrease as frequency increases. This indicates excellent barrier properties and capacitive behavior characteristic of an undamaged coating. This is a characteristic response of the highly capacitive coating. The large and small holiday defects display much lower impedance values, with a large drop in overall impedance values and more positive phase angle values. Small holidays consistently show higher impedance values than large holidays across all protection potentials, suggesting better residual protection capabilities. As for the protection potential effect, OCP shows baseline behavior, whereas standard protection provides optimal results for defect mitigation. Both

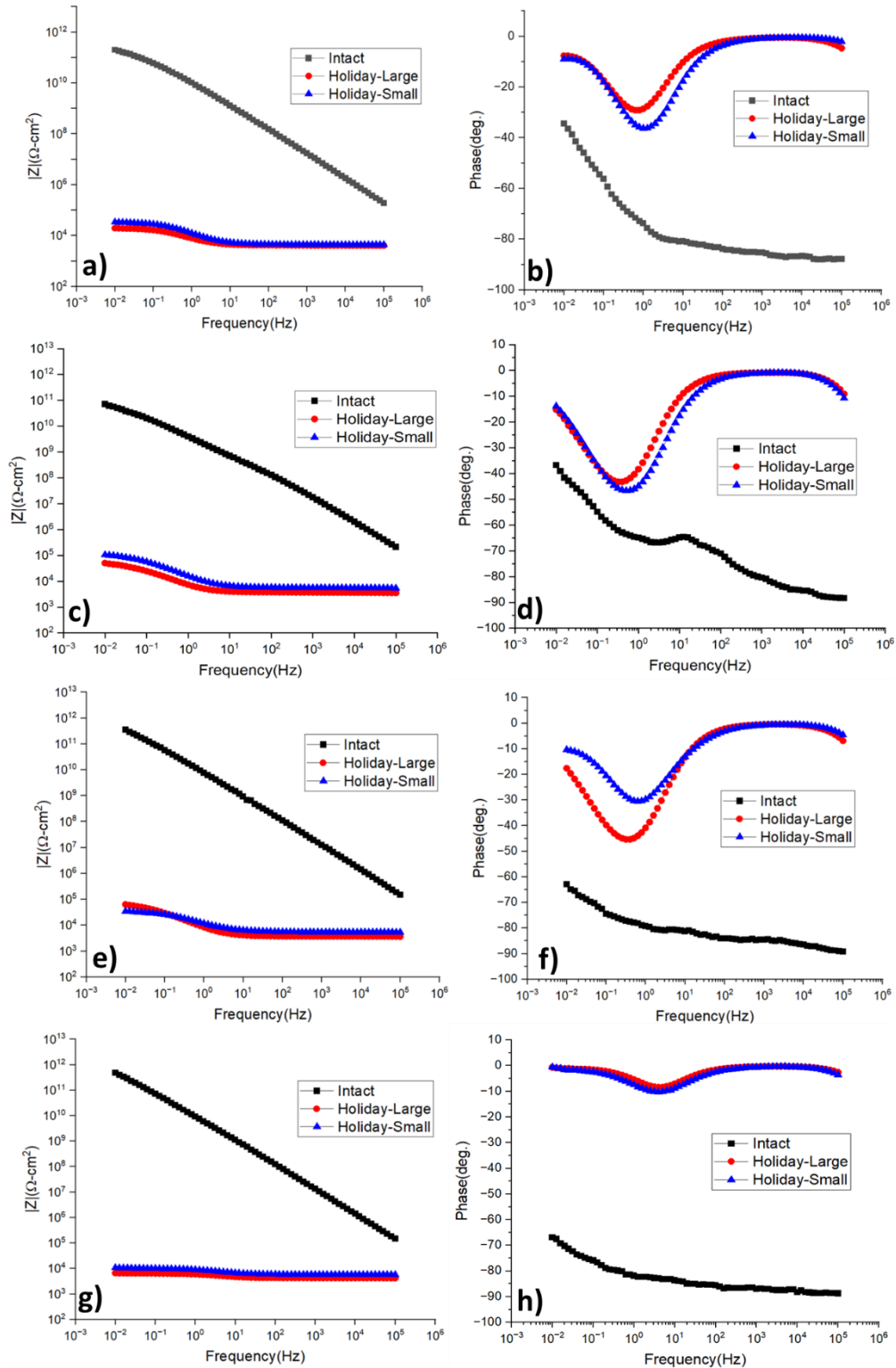
defect sizes show distinctive phase angle peaks in the mid-frequency range ( $10^0$ - $10^2$  Hz) when tested at OCP. For under protection, small holiday shows deeper phase angle minima ( $-40^\circ$ ) and large holiday exhibits shallower phase angle response ( $-20^\circ$ ). Under standard protection, phase angle minima become more pronounced for both defect sizes. Small holidays show more negative phase angles than large holidays. For overprotection, phase angles become less negative, and there is a convergence of phase response between large and small holidays. This reduction in phase angle variation shows more resistive behavior.



**Figure 4:** Bode and phase angle plots for FBE coatings with and without holidays for various CP conditions (a-b) open circuit conditions, (c-d) under protection, (e-f) standard protection, and (g-h) over protection

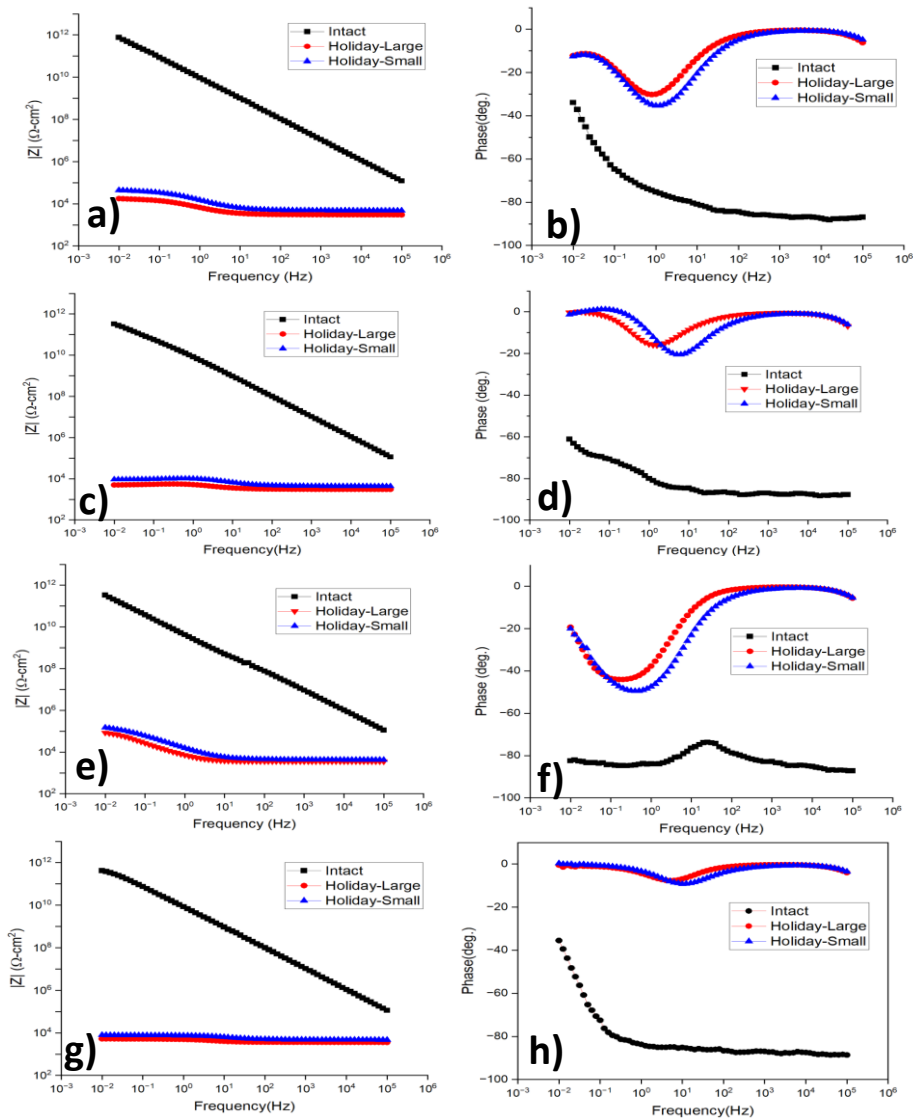
Figure shows the effect of polarization condition on the impedance response of coal tar coatings with and without holidays present in the coating. The intact coating shown consistently high impedance ( $10^{10}$ - $10^{12}$   $\Omega$ -cm<sup>2</sup>) at low frequencies similar to FBE. These high values were shown for each polarization condition as well. The phase angle behavior for intact coating exhibits near-capacitive behavior approaching  $-90^\circ$  and shows minimal frequency dependence in mid to high frequency ranges. Defect responses in coal tar show clearer separation between the intact and damaged coating conditions. Applying the under protection potential for the coal tar coating defects did not produce drastic change from the OCP conditions. But, applying standard protection did increase the overall impedance relative to under protection potential and OCP conditions. For the over protection potential the overall impedance did drop but is most likely due to the higher rate of cathodic reaction occurring with the larger more negative potential that was applied to the surface.

The overall impedance response was very similar for the two coatings when various cathodic protection potentials were applied. The intact coatings showed large impedance values and phase angle values near  $-90^\circ$  for most of the frequency domain regardless of the potential application. There was little difference between the impedance response between OCP and under protection potential for FBE and coal tar coatings. This is most likely due to OCP and under protection potential being similar in magnitude. Impedance measurements under the standard protection potential did show an increase in the impedance magnitude and more negative phase angle values for both small and large holidays. This is indicative that the exposed surface was more protected with the application of the standard protection potential. For both FBE and coal tar coatings when the overprotection potential was applied the impedance magnitude decreased and phase angle values became more positive. This is most likely due to the increased cathodic reaction rate with a more negative potential relative to the other three conditions.



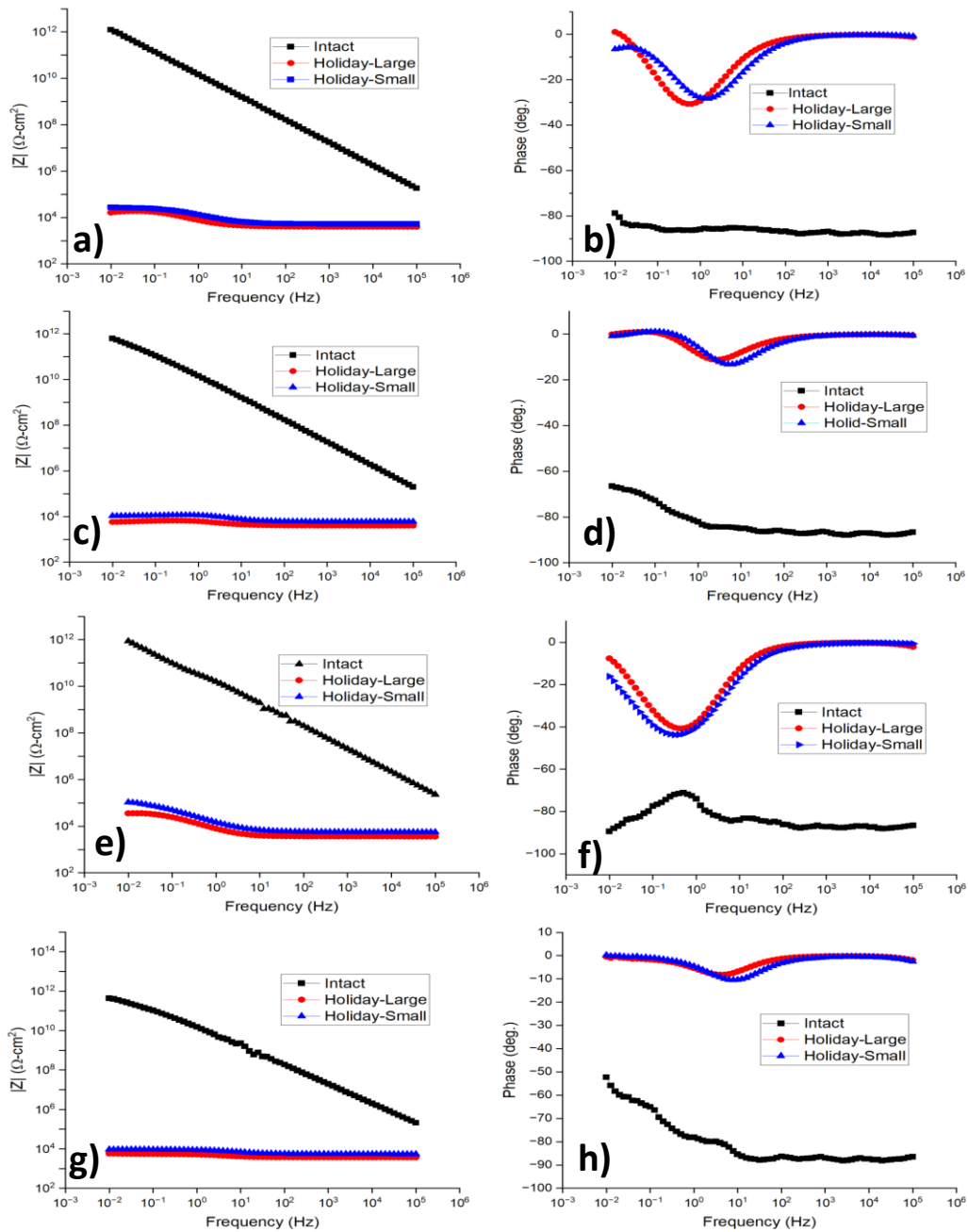
**Figure 16:** Bode and phase angle plots for Coal Tar coatings with and without holidays for various CP conditions (a-b) open circuit conditions, (c-d) under protection, (e-f) standard protection, and (g-h) over protection

Figure 17 presents the Bode and phase angle plots for a 4500 coating with a thickness of 25 mils under various CP conditions. The intact coating maintains high impedance values at low frequencies, like other coatings, indicating strong barrier properties. Defect responses show a notable decrease in impedance compared to intact coatings, with small holidays generally exhibiting higher impedance than large ones. Under standard protection, impedance increases, and phase angles become more negative, suggesting enhanced protection of the exposed surface. Overprotection leads to decreased impedance and less negative phase angles, indicating increased cathodic activity. The plots suggest that standard protection is most effective for mitigating defects in these coatings.



**Figure 17:** Bode and phase angle plots for 4500 coating (25 mils thickness) coatings with and without holidays for various CP conditions (a-b) open circuit conditions, (c-d) under protection, (e-f) standard protection, and (g-h) over protection

Figure 18 shows similar trends for 4500 coating with a thickness of 40 mils. The thicker coating maintains high impedance at low frequencies, consistent with other coatings. Defect responses are more pronounced, with small holidays showing higher impedance than large ones across all protection conditions. Standard protection enhances impedance and phase angle responses, indicating better defect mitigation. Overprotection results in decreased impedance and less negative phase angles, likely due to increased cathodic reactions. The thicker coating may offer slightly better barrier properties, but the overall trends are consistent with thinner coatings.



**Figure 18:** Bode and phase angle plots for 4500 coating (40 mils thickness) coatings with and without holidays for various CP conditions (a-b) open circuit conditions, (c-d) under protection, (e-f) standard protection, and (g-h) over protection

All three coatings exhibit high impedance values at low frequencies when intact, indicating strong barrier properties. Standard protection generally enhances impedance and phase angle responses, suggesting better defect mitigation. Overprotection leads to decreased impedance and less negative phase angles due to increased cathodic reactions. The coal tar coatings show clearer separation between intact and damaged conditions compared to FBE coatings. The 4500 coating, regardless of thickness, follows similar trends to the other coatings but may offer slightly better barrier properties due to its thickness. Overall, standard protection is most effective for mitigating defects in these coatings.

## **Future Work**

Future work will continue using the NS4 solution as the standardized testing medium due to its proven effectiveness in simulating soil-like environments. Upcoming studies will extend testing to cover both acidic and neutral pH conditions in more controlled and diverse configurations to better represent real-world variability. The use of NS4 across these pH ranges will enable a systematic understanding of how pH fluctuations affect corrosion behavior and coating performance. Additionally, we will implement solution deaeration protocols using varied gas purging techniques (e.g., N<sub>2</sub>, CO<sub>2</sub> blends) to simulate different oxygen availability scenarios, further refining our understanding of electrochemical responses under near-anoxic conditions. A critical future direction involves de-aerating the solution performance across coatings of different types and thicknesses, as documented in this report (e.g., coal tar, FBE, yellow jacket, 4500, tri-layer systems, etc.). This de-aerating process will help quantify the protection efficiency relative to coating characteristics under identical exposure conditions. Coating thickness ranging from 10 to 50 mils—will be further evaluated in conjunction with coating integrity states (intact, small holiday, large holiday, and delamination). By integrating the effects of pH, deaeration, coating material, and thickness, we aim to establish a comprehensive electrochemical database that enhances corrosion prediction models and supports the optimization of cathodic protection systems in buried pipeline scenarios.